Damage Diagnostics of a Composite Single-Stiffener Panel Under Fatigue Loading Utilizing SHM Data Fusion

Agnes A. R. Broer[1(✉)], Georgios Galanopoulos[2], Dimitrios Zarouchas[1], Theodoros Loutas[2], and Rinze Benedictus[1]

[1] Structural Integrity and Composites Group, Faculty of Aerospace Engineering, Delft University of Technology, Kluyverweg 1, 2629HS Delft, The Netherlands
A.A.R.Broer@tudelft.nl

[2] Laboratory of Applied Mechanics and Vibrations, Department of Mechanical Engineering and Aeronautics, University of Patras, 26500 Rio, Greece

Abstract. A case study is presented in which the first steps are made towards the development of a structural health monitoring (SHM) data fusion framework. For this purpose, a composite single-stiffener panel is subjected to compression-compression fatigue loading (R = 10). The carbon-epoxy panel contains an artificial disbond of 30 mm, which was created using a Teflon insert during manufacturing and placed between the skin and the stiffener foot. Under the applied fatigue load, the disbond is expected to grow and its propagation is monitored using two SHM techniques, namely acoustic emission (AE) and Rayleigh-scattering based distributed fiber optic strain sensing. Four AE sensors are placed on the skin, thereby allowing for disbond growth detection and localization. On each stiffener foot, fiber optic sensors are surface-bonded to monitor the growth of the disbond under the applied fatigue loading. The distributed strain measurements are used to localize and monitor the disbond growth. The strength of each technique is utilized by fusing the data from the AE sensors and the fiber optic sensors. In this manner, a data-driven approach is presented in which a data fusion of the different techniques allows for monitoring the damage in the stiffened panel on multiple SHM levels, including disbond growth detection and localization.

Keywords: Data fusion · Acoustic emission · Distributed strain sensing · Composite single-stiffener panel · Fatigue loading

1 Introduction

Stiffened composite skin panels are commonly used in the aircraft industry and when used in-service, the occurrence of damage is inevitable. These damages can be caused by operational loads and environmental conditions or caused by an unexpected event such as a foreign object impact. Currently, commercial

P. Rizzo and A. Milazzo (Eds.): EWSHM 2020, LNCE 127, pp. 616–625, 2021.
https://doi.org/10.1007/978-3-030-64594-6_60

aircraft do not include permanently installed sensors to monitor damage initiation and propagation, resulting in the need for manual inspections. By placing a sensor network, the health of the structure can be monitored at all moments. In order to fulfill the diagnostic requirements, information is required on multiple structural health monitoring (SHM) levels, i.e. 1) detection, 2) localization, 3) type, and 4) size. Many SHM techniques are available for this purpose, such as acoustic emission (AE), lamb waves (LW), and static and dynamic strain sensing. Two techniques will be used in this work: AE and distributed fiber optic sensing (DFOS). As will be seen next, each technique has its strengths and their combination can potentially allow for a damage diagnostic on multiple SHM levels.

AE can be used to monitor the damage initiation and propagation in a composite, as well as for damage localization and damage type identification. Damage localization can be achieved when multiple sensors are used simultaneously in a cooperative fusion setting, followed by the application of an algorithm such as the time-of-arrival technique. Yet the error of localization might be large, especially for an anisotropic medium such as a composite panel, since the wave velocity is dependent on the propagation direction. Other methods have been proposed to resolve this disadvantage, such as the Delta T-Mapping approach [1,3,4,11] or by employing a close sensor placement that allows an assumption of constant wave velocity [2,9]. Though reducing the localization error, the Delta T-Mapping approach is user-intensive, as well as structure- and lay-up-dependent due to its manual mapping, while the second approach requires a larger number of sensors. Damage type can be identified by clustering AE feature data, yet it is not commonly seen in stiffened panels, which are the focus of this work. Generally, classification techniques are applied on a coupon level and the results are affected by overlapping feature values (overview given in [6,12]). Though an example of damage type identification on a panel level is shown by Kolanu et al. [8] who categorized AE feature data obtained from a single-stiffened carbon fiber-reinforced polymer (CFRP) panel in (post-)buckling.

DFOS can be used to monitor the strain at the location of the fiber placement. Rayleigh-scattering based distributed fiber optic strain sensing provides a distributed strain measurement along the length of the fiber with intervals as low as 0.65 mm [10], as opposed to Fiber Bragg Gratings (FBGs) that provide point strain sensing. Strain measurements are affected by different sources, e.g. the applied load and the presence of damage, noise, or vibrations. If the influence of the damage on the strain measurement can be identified, it can be used for damage diagnostics. For example, the distributed strain measurements can be employed for the detection and the localization of impact damage in stiffened composite panels [14]. Furthermore, the disbond growth rate under fatigue loading can potentially be sized using distributed strain measurements [13].

Each monitoring technique has its strengths and only provides information about certain SHM levels. In this work, it is hypothesized that a fusion of sensor data from AE and DFOS will release synergistic effects that can result in an improved damage diagnostic on multiple SHM levels. In this view, AE can

be used for damage detection and localization, while strain measurements from DFOS can be employed to localize and monitor disbond growth at the stiffener. The first steps in testing the hypothesis are made in the presented case study. A composite single-stiffener panel with an artificial disbond of 30 mm is tested in compression-compression fatigue until failure and monitored using AE sensors and DFOS. It is shown that their data can be fused to describe the damage process throughout the test until the final failure. In the next section, the experimental campaign is described, including details on each monitoring technique. Section 3 presents a data fusion of the different SHM techniques and describes the damage propagation per cycle period by simultaneously looking at damage detection, localization, disbond growth, as well as growth direction.

2 Experimental Campaign

A test campaign took place at the TU Delft Aerospace Structures and Materials Laboratory in November and December 2019 as part of the H2020 ReMAP project.[1] During this test campaign, a composite skin-stiffener panel was tested in compression-compression (C-C) fatigue loading. The panel, based on a design by Embraer and shown in Fig. 1, consists of a skin panel and a single T-stiffener. Both the skin and the stiffener are made from IM7/8552 carbon fiber-reinforced epoxy unidirectional prepreg and its lay-ups are $[45/-45/0/45/90/-45/0]_S$ and $[45/-45/0/45/-45]_S$, respectively. During manufacturing, which was performed by Optimal Structural Solutions, an artificial disbond of 30 mm was created by placing a Teflon film between the right stiffener foot and the skin. Additionally, two resin blocks were added to ensure a distributed load introduction. The panel's dimensions, as well as the location of the disbond, are indicated in Fig. 1c.

Six monitoring techniques were used to monitor the damage growth in the panel, namely (1) AE, (2) DFOS, (3) FBGs, (4) Lamb Wave Detection System (LWDS), (5) Digital Image Correlation (DIC), and (6) Camera. For the scope of this paper, only data from the AE system and DFOS is used to monitor the health of the panel, hence the remainder of this work will focus on these techniques.

As previously stated, the panel was loaded in C-C fatigue loading with an R-ratio of 10 and a frequency 2 Hz. Initially, the fatigue load was set at a minimum load of −5.0 kN and a maximum load of −50.0 kN. After 100,000 cycles, the load was increased to a minimum load of −6.0 kN and a maximum load of −60.0 kN, while the R-ratio and frequency were kept constant. These load levels were maintained until the final failure of the panel, i.e. when the panel lost its load-bearing capability.[2] The fatigue load was interrupted at certain intervals to allow for measurements by the SHM systems. The load cycle pattern is as follows and repeats itself every 5000 cycles. Every 5000 cycles, the applied load

[1] ReMAP: Real-time Condition-based Maintenance for Adaptive Aircraft Maintenance Planning. https://h2020-remap.eu/.

[2] The test was interrupted at 30,000, 50,000, 70,000, 100,000, and 245,000 for limited time periods.

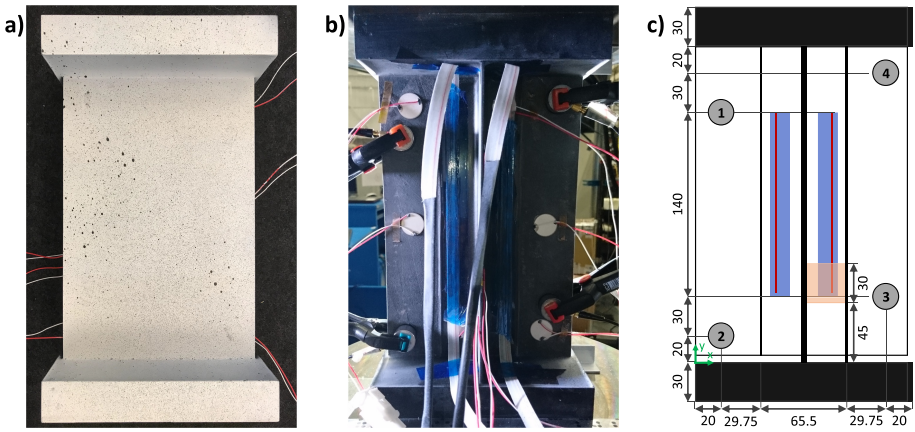

Fig. 1. Single stiffener panel as seen from (a) skin and (b) stiffener side. Its dimensions in [mm] and the sensor locations are shown in (c), where the AE sensors are indicated as gray circles, the two optical fibers as red lines inside the SMARTape (blue), and the Teflon film as an orange square.

is reduced to 0 kN[3] to allow for the LW measurements. Every 500 cycles (except for the 5000th cycle), a quasi-static (QS) load is applied from the minimum to the maximum load (either from −5.0 kN to −50 kN or from −6.0 kN to −60 kN) with a displacement rate of 0.5 mm/min. During the QS loading, measurements are taken by several techniques, namely by the DIC system, camera system, DFOS, and FBGs. The DFOS system records a strain measurement both at the minimum and maximum of the QS load and the AE system records continuously throughout the test. The latter two SHM systems are discussed in more detail next.

Acoustic Emission. The AE sensors are VS900-M broadband sensors from Vallen Systeme GmbH with an operating frequency range of 100–900 kHz. An AMSY-6 Vallen acquisition system is used to record the AE hits. Four AE sensors are clamped on the panel in different locations to form a parallelogram and allow for damage localization. The [x, y] location of sensor 1, 2, 3, and 4 is [20.0, 190.0], [20.0, 20.0], [145.0, 50.0], and [145.0, 220.0] mm, respectively, and is also displayed in Fig. 1c.

To prevent the capturing of noise signals, an amplitude threshold of 50 dB was set for recording of the hits. For localization, the internal Vallen processor for planar location was employed, which is based on Geiger's method [5]. After testing, it was seen that the AE system localized a large number of signals, therefore an amplitude filter of 80 dB was applied to the localized events. Additionally, a filter was implemented to remove events with a location uncertainty

[3] The load level was changed to −0.2 kN after 50,000 cycles.

higher than 50 mm. Lastly, only localized events within the AE sensor region are considered.

Distributed Fiber Optic Sensing. An optical fiber sensor has been placed inside a SMARTape [7], which was adhesively bonded to the surface of the stiffener foot using a co-polyamide-based adhesive. Two SMARTapes were used: one on each stiffener foot. Due to the placement of one piezoelectric transducer (PZT) on each stiffener foot, strain measurements are only available for part of the stiffener foot's length as indicated in Fig. 1c. The strains were measured using a LUNA ODiSI-B Optical Distributed Sensor Interrogator with an acquisition rate of 23.8 Hz and a gauge pitch of 0.65 mm. Since the interrogator consists of only 1 interrogation channel, the two SMARTapes were spliced together. Additionally, a coreless fiber was added at the end of the fiber to minimize reflections. Note that the distributed strain measurements required no post-processing procedures such as filtering or smoothing.

3 Damage Monitoring Results

Based on the findings, the test has been split into different cycle periods to allow for discussion in this section. For each considered cycle period, the localized AE events are presented in Fig. 2. Moreover, the cumulative energy of all recorded AE hits is shown in Fig. 3, where bins of 5000 cycles have been adopted. Here, in contrast to the localization, no filtering was applied. The strain measurements at the surface of the left and right stiffener foot are presented in Fig. 4a and b, respectively, for different cycle numbers. These correspond to the start and end of each cycle period. Note that due to the LW measurements every 5000 cycles, the strains were not recorded at these intervals and the subsequent strain measurements are shown instead. In the next subsections, the damage propagation in the stiffened panel will be discussed based on the AE and strain data and the defined cycle periods.

0–100,000 Cycles. The strain measurements on the stiffener feet at 500 and 99,500 cycles are displayed in Fig. 4a and b, while the localized AE events for a similar cycle period are shown in Fig. 2a. Both measurements do not show indications of damage growth during this cycle period. Moreover, the cumulative energy of the AE hits has only shown a minimal increase from 0 to 100,000 cycles. The latter, together with the identification of a minimal strain reduction along the lengths of both stiffener feet, can be an indication that only stiffness degradation took place under the fatigue loading rather than disbond growth.

100,000–210,000 Cycles. Figure 4a and b show comparisons between the strain measurements on the stiffener feet at 100,500 and 210,500 cycles. The compressive strain in both feet has increased at 100,500 with respect to 99,500 cycles due to the increased maximum load (−50 kN to −60 kN). Comparing the

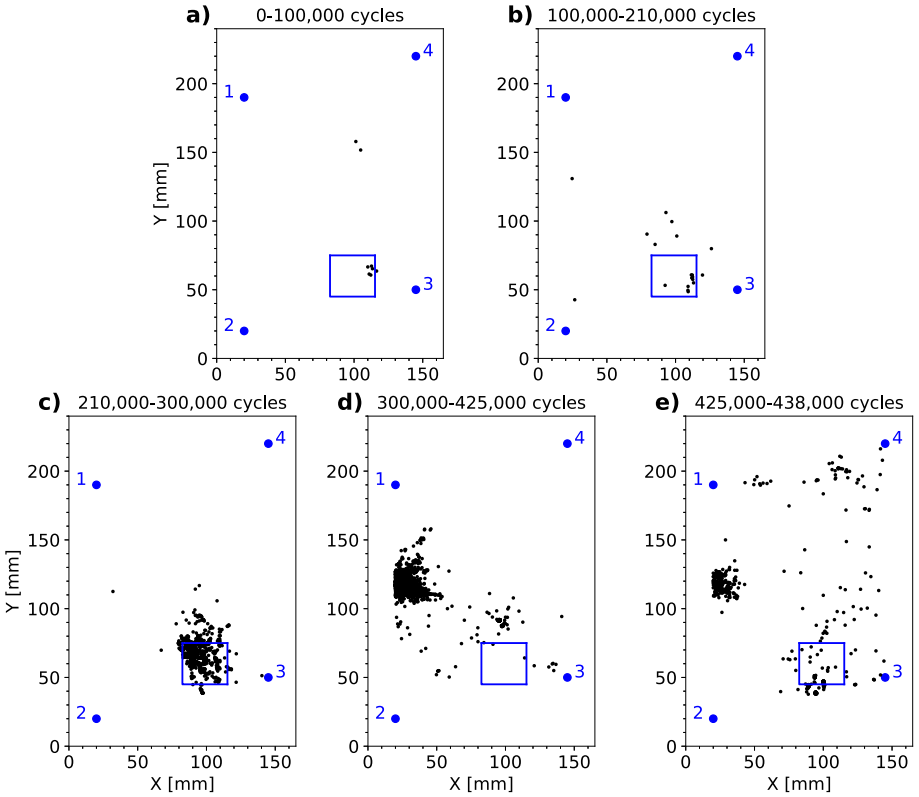

Fig. 2. Localized acoustic emission hits for specified cycle periods. The initial disbond location is indicated by a blue square and the AE sensors by blue circles.

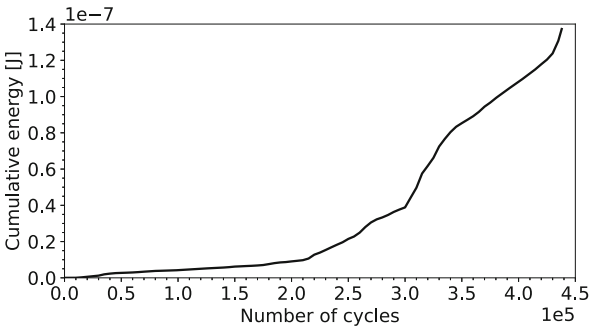

Fig. 3. AE cumulative energy versus number of cycles, with bins of 5000 cycles.

strain measurements at 100,500 and 210,500 cycles, little change is detected on the left foot, while the right foot shows a larger reduction in compressive strain. However, this reduction in strain does not occur with a similar rate at

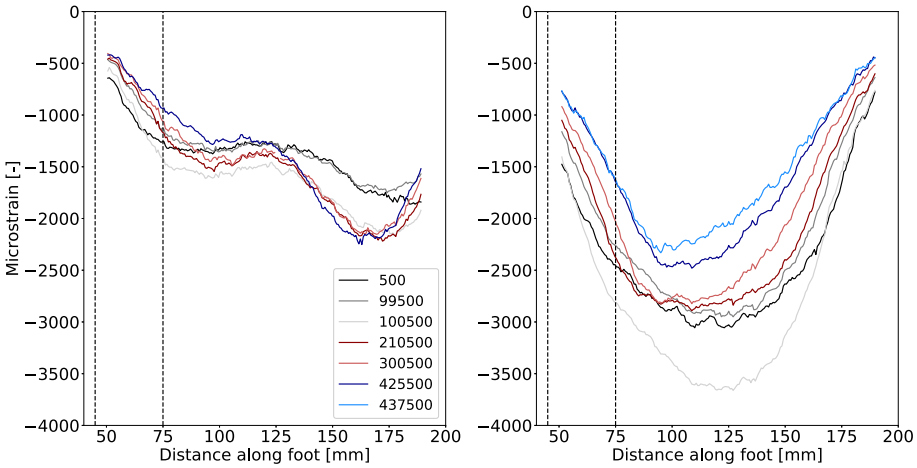

(a) Left stiffener foot (b) Right stiffener foot

Fig. 4. Surface strain measurements along the stiffener feet. The disbond is located in the right stiffener foot and its initial location is indicated in both graphs using black dashed lines. Legend is similar for both figures.

all locations: the bottom region below a height of 90 mm shows a smaller absolute compressive strain reduction than the region above 90 mm. Evaluating the localized AE events for this cycle period (Fig. 2b), it is seen that some hits are localized around the disbond region. Figure 3 shows a further increase in cumulative energy, although it is a slightly steeper increase than in the previous cycle period. These results are an indication that, besides stiffness degradation, activity is present near the disbond resulting in disbond growth.

210,000–300,000 Cycles. Between 210,000 and 300,000 cycles, many AE events are localized, which are centered in the initial disbond area and above it (Fig. 2c). Furthermore, the cumulative energy curve (Fig. 3) has an increased slope and increases continuously throughout the considered period. The distributed strain measurements along the stiffener feet for 210,500 and 300,500 cycles are shown in Fig. 4a and b. Similar to the previous cycle period, the left stiffener foot experiences only minimal changes in strain values while the right stiffener foot shows larger differences: a small strain reduction is seen between 80 mm and 110 mm, while the region above 110 mm displays larger reductions in strain. Based on the results from both SHM techniques, it can be concluded that the disbond has grown during the considered cycle period. In addition, the direction of disbond growth can be derived from the results and it is believed to have grown upward along the length of the right stiffener. This is based on the concentration of AE events in the upper region and above the initial disbond area, as well as the minimal strain reduction on the right stiffener foot between

80 mm and 110 mm. Lastly, based on the strain reduction above the disbond region, it is believed that further stiffness degradation took place.

300,000–425,000 Cycles. As little AE events are localized in the vicinity of the disbond region and the strain distribution on the right stiffener foot shows a constant reduction in strain over its length, it is expected that the disbond did not further grow between 300,000 and 425,000 cycles. Yet further stiffness degradation occurred as indicated by the reduced compressive strain in the right stiffener foot.

Nevertheless, it needs to be recognized that a large number of AE events is localized in the center height of the left skin. Moreover, the cumulative energy increases rapidly after 300,000 cycles. Evaluating the left stiffener foot, only a minimal compressive strain reduction is noted in the lower half, thereby providing little clarification on the cause of these AE events. Therefore, data from two additional SHM techniques was evaluated, namely the DIC system and LWDS. Neither provided indications of damage initiation and propagation. Given that a PZT of the LWDS is located at [x, y] = [25.0, 120.0] mm, it is therefore argued by the authors that these AE hits do not indicate a damage process but that these were instead caused by an external source. A further investigation is required to establish the actual cause; however, it is hypothesized to be either a faulty PZT or a mechanical process such as the cable of the PZT hitting the panel during fatigue loading.

425,000–438,000 Cycles. Evaluating results closer to final failure, it is seen that the strain distribution in the lower half of the right stiffener foot remains close to constant, while the region above 90 mm shows a further strain reduction. Simultaneously, the left stiffener shows a reduction in compressive strain between approximately 100 mm and 130 mm while the strain in the lower and upper regions remains close to constant. The latter might be caused by either a disbond growth upward along the right stiffener or by a disbond growth from the right stiffener foot to the left stiffener foot. This reasoning can be further substantiated when evaluating the localized AE events (Fig. 2e); events are localized both below and above the initial disbond region. Additionally, around a height of y = 60 mm, multiple AE events are localized left of the disbond area. The growth of the disbond across the length of the stiffener as well as along its width is believed to have resulted in the final failure of the panel. The panel failed after 438,000 cycles during QS loading.

4 Conclusions

The first steps towards the development of an SHM data fusion framework were presented by means of a case study consisting of a composite single-stiffener panel with an artificial disbond of 30 mm. It was shown that the disbond growth under fatigue loading can be monitored by fusing AE data with DOFS strain

measurements on the stiffener feet. The combination of the two techniques allows for a damage assessment on multiple SHM levels at different moments throughout the loading cycle. The AE hits allowed for detection and localization of the damage in the panel. The strain measurements from the DOFS allowed for monitoring the disbond growth, as well as the identification of stiffness degradation. By fusing the different datasets, an improved assessment of disbond growth was obtained, which additionally allowed for indicating the disbond growth direction.

Although this work shows the first advantages of fusing SHM data for damage diagnostics, it also displays that two SHM techniques might not be sufficient to monitor the health of a stiffened skin panel under fatigue loading; additional techniques, namely digital image correlation (DIC) and LW measurements, were needed to investigate the source of localized AE events in the skin. Moreover, it was not yet possible to obtain a quantitative estimate of the disbond growth rate using just two techniques. The latter will require further investigation, for example with the assistance of additional SHM techniques or by training a sizing algorithm. Though several areas require further investigation, the presented study shows the benefits of fusing SHM data in a data-driven approach, thereby resulting in an improved damage diagnostic on multiple SHM levels.

Acknowledgements. We would like to acknowledge Embraer for the design of the SSCs, Optimal Structural Solutions for the manufacturing of the SSCs, Smartec for the SMARTapes procurement, Cedrat Technologies for the LW sensing equipment, École Nationale Supérieure d'Arts et Métiers for the LW data acquisition software, and our colleagues at the labs of TU Delft and University of Patras for their technical support. This work was financially supported by the European Union's Horizon 2020 research and innovation program under grant agreement No. 769288.

References

1. Baxter, M.G., Pullin, R., Holford, K.M., Evans, S.L.: Delta T source location for acoustic emission. Mech. Syst. Signal Process. **21**, 1512–1520 (2007)
2. Ciampa, F., Meo, M.: A new algorithm for acoustic emission localization and flexural group velocity determination in anisotropic structures. Compos. Part A: Appl. Sci. Manuf. **41**, 1777–1786 (2010)
3. Eaton, M.J., Pullin, R., Holford, K.M.: Acoustic emission source location in composite materials using Delta T mapping. Compos. Part A: Appl. Sci. Manuf. **43**, 856–863 (2012)
4. Eaton, M.J., Pullin, R., Holford, K.M.: Towards improved damage location using acoustic emission. J. Mech. Eng. Sci. **226**, 2141–2153 (2012)
5. Ge, M.: Analysis of source location algorithms. Part II: iterative methods. J. Acoust. Emission **21**, 29–51 (2003)
6. de Groot, P.J., Wijnen, P.A.M., Janssen, R.B.F.: Real-time frequency determination of acoustic emission for different fracture mechanisms in carbon/epoxy composites. Compos. Sci. Technol. **55**, 405–412 (1995)
7. Inaudi, D., Glisic, B.: Development of distributed strain and temperature sensing cables. In: Voet, M., Willsch, R., Ecke, W., Jones, J., Culshaw, B. (eds.) 17th International Conference on Optical Fibre Sensors, vol. 5855, pp. 222–225. International Society for Optics and Photonics, SPIE (2005)

8. Kolanu, N.R., Raju, G., Ramji, M.: Experimental and numerical studies on the buckling and post-buckling behavior of single blade-stiffened CFRP panels. Compos. Struct. **196**, 135–154 (2018)
9. Kundu, T., Nakatani, H., Takeda, N.: Acoustic source localization in anisotropic plates. Ultrasonics **52**, 740–746 (2012)
10. Luna ODiSI-B: Optical Distributed Sensor Interrogator Model ODiSI-B: User's Guide. Luna Inc. (2017)
11. Pearson, M.R., Eaton, M.J., Featherston, C.A., Pullin, R., Holford, K.M.: Improved acoustic emission source location during fatigue and impact events in metallic and composite structures. Struct. Health Monit. **16**, 382–399 (2017)
12. Raju, Azmi, A.I., Prusty, B.G.: Acoustic emission techniques for failure characterisation in composite top-hat stiffeners. J. Reinf. Plast. Compos. **31**, 495–516 (2012)
13. Ribeiro, F.N., Martinez, M., Rans, C.: Evaluation of mode II fatigue disbonding using Central Cut Plies specimen and distributed strain sensing technology. J. Adhes. **95**, 259–285 (2019)
14. Tur, M., Bosboom, M.B., Evenblij, R., Michaelides, P., Gorbatov, N., Bergman, A., Ben-Simon, U., Kressel, I., Kontis, N., Koimtzoglou, C.: Fiber-optic based HUMS concept for large aircraft structure based on both point and distributed strain sensing. In: 8th European Workshop on Structural Health Monitoring (2016)